JOURNAL OF CATALYSIS 148, 534–539 (1994)

A High-Resolution TEM Study of the Annealing of Pd Particles Supported on MgO

S. Giorgio, C. R. Henry, C. Chapon, and C. Roucau*

*CRMC2-CNRS, Campus de Luminy, Case 913, F-13288 Marseille Cédex 9, France; and *CEMES LOE CNRS 29, Rue Jeanne Marvig, B.P. 4347, F-31055 Toulouse Cédex, France*

Received October 6, 1993; revised March 30, 1994

Pd clusters (4–5 nm) epitaxially grown on clean surfaces of MgO microcubes were annealed at 450°C in pure O_2 or H_2 at pressures of 10^{-7} and 10^{-1} Torr. The samples were investigated by high-resolution transmission electron microscopy in order to image both the profile view and the interface Pd/MgO. Particles annealed in oxygen at 10^{-7} Torr develop a slightly rounded shape. Their lattice parameter is expanded by 2%, as in the case of the same clusters annealed in vacuum. Annealing under a higher pressure of oxygen induces a full rounded shape and produces PdO on the surface and edges of the Pd particles. Particles annealed in H_2 retain the shape of a half-octahedron truncated at the top by (100) faces and their lattice parameter is dilated by 3–4%. © 1994 Academic Press, Inc.

INTRODUCTION

The catalytic activity of small metallic particles supported on a substrate is related to their size, shape, possible surface reconstruction, and interaction with the substrate.

The equilibrium shape of polyhedral particles can be calculated from the minimization of the Gibbs surface free energy of the crystal according to the Wulff theorem (1). However, for particles smaller than 2 nm, the contribution of the edges to the surface free energy is not negligible, and the Wulff theorem is not applicable (2, 3). The surface tension of the different faces is always modified by the adsorption of foreign molecules. Gases chemisorb more strongly on faces with a low atomic density; it is believed that chimisorption lowers the surface free energy and then reduces the anisotropy in the crystal shape (4, 6). Thus gas adsorption on the faces of a particle is able to modify the particle shape and modify their catalytic activity.

Variations of the morphology of crystals due to gas exposure have been experimentally and theoretically studied, especially for Pt and Pd crystals and alloys. The role of oxidation or reduction treatments by O_2, H_2S, H_2, CO, on the formation of (111) and (100) facets on Pt particles has been extensively studied (5–12).

Similar studies of the interaction of CO, O_2, N_2, and H_2 were carried out on supported Pd particles (13–20). Exposure to CO or N_2 does not significantly change the morphology of Pd particles supported on MgO or mica (14). However, in the case of O_2, from the top view of the TEM images of particles, it has been concluded that most of the particles are flattened and have coalesced. This flattening is explained by a variation of the surface free energy of the Pd particles (σ_{Pd}) due to the gas adsorption (13). On the other hand, the surface free energy σ_{MgO} and the interfacial energy $\sigma_{Pd/MgO}$ does not vary. Larger effects were found for Pd particles exposed to the air (14), such as coalescence and rounding of the particles.

In the case of Pd on mica, the co-adsorption of CO and O_2 was found to change the morphology and epitaxial orientation of the particles on the substrate (16).

On MgO, the full oxidation of (001)-oriented Pd particles to PdO resulted in (110)-oriented PdO particles in epitaxy on the MgO with [001]PdO // [001]MgO and (110)Pd // (110)MgO (17).

This paper reports on the equilibrium shape and the structure of Pd particles (<6 nm) supported on MgO after *in situ* annealing under O_2 or H_2.

EXPERIMENTAL

Pd particles have been epitaxially grown under UHV by vapor condensation on clean MgO microcubes in order to observe the particles both in top view and in profile view, according to the technique described previously (21, 22). Thereafter, the samples have been annealed *in situ* in the vacuum chamber under an O_2 or H_2 atmosphere at 10^{-1} and 10^{-7} Torr.

Sample Preparation

MgO cubes were synthesized by burning Mg ribbon in a mixture of pure gases (20% O_2 + 80% N_2) at 1 atm in the vacuum chamber. They were collected on a microscope grid coated with a carbon layer (21) and mounted

0021-9517/94 $6.00

on an oven. For the present experiments, the chamber was modified in order to improve the vacuum. The chamber was evacuated to a pressure of 7×10^{-10} Torr. The sample was heated at 450°C and brought in front of a Knudsen cell for the Pd condensation at a flux of 1×10^{13} atoms cm^{-2} s^{-1}, under a residual pressure lower than 5×10^{-9} Torr. Then, pure O_2 or H_2 was introduced into the chamber at different pressures (10^{-7} or 10^{-1} Torr). The samples were annealed at 450°C in the gases during 1 h.

Before transfer to the microscope, the samples were covered *in situ* by a carbon layer, at room temperature to avoid contamination in the ambient atmosphere.

High-Resolution Transmission Electron Microscopy

The samples were observed with a Philips CM 30 microscope, operating at 300 kV and equipped with super twin polar pieces. Figure 1 is an overview of the Pd particles on the MgO cubes.

The particles are (100) oriented on MgO (21). Therefore, in the high-resolution transmission electron microscopy (HRTEM) images,the (200) and (020) lattice fringes of Pd and MgO are visible. All the images were recorded at a magnification of 600,000. The areas containing a particle seen in profile view on the MgO were digitized with 256 grey levels and 768×512 pixels, corresponding to a sampling of 1 pixel for 0.013 nm at the level of the sample. Then, the lattice distances between the (200) planes normal to the interface were measured in different parts of the particles (at the interface, in the volume, and near the top), according to the method previously described (22). For all measurements of the Pd lattice, the MgO lattice was taken as an internal calibration.

RESULTS

Annealing Under Oxygen

Figure 2 shows a high-resolution image of several Pd particles annealed in O_2 at 10^{-7} Torr in profile view. All the particles are slightly rounded. The interface is flat, and the top of the particles is somewhat distorted.

The intensity profiles were recorded along the [100] directions parallel to the interface in each Pd layer, from the interface towards the top. However, as the top of the particles is not as well defined as in the case of particles annealed in the vacuum, the measurements are only made until the 8th layer, in particles containing about 12 layers.

Figure 3 shows the average variations of the lattice parameter of 4- to 5-nm Pd particles annealed in 10^{-7} Torr of O_2, with a precision of ± 0.014 nm. The first layer is accommodated to the MgO substrate, then the lattice parameter reaches a value corresponding to the bulk Pd lattice expanded by 2%. This is the same dilatation as was measured in Pd particles of the same size (4 nm) annealed under UHV (21).

Figure 4 shows a Pd particle obtained by annealing in 10^{-1} Torr of oxygen. The position of the Pd/MgO interface

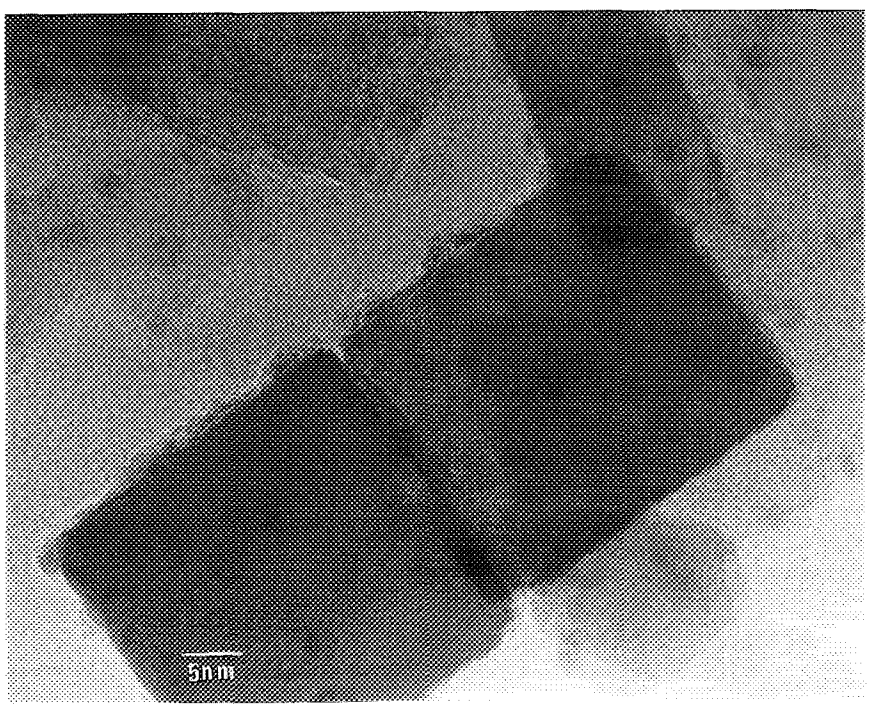

FIG. 1. General view of MgO microcubes covered with Pd particles.

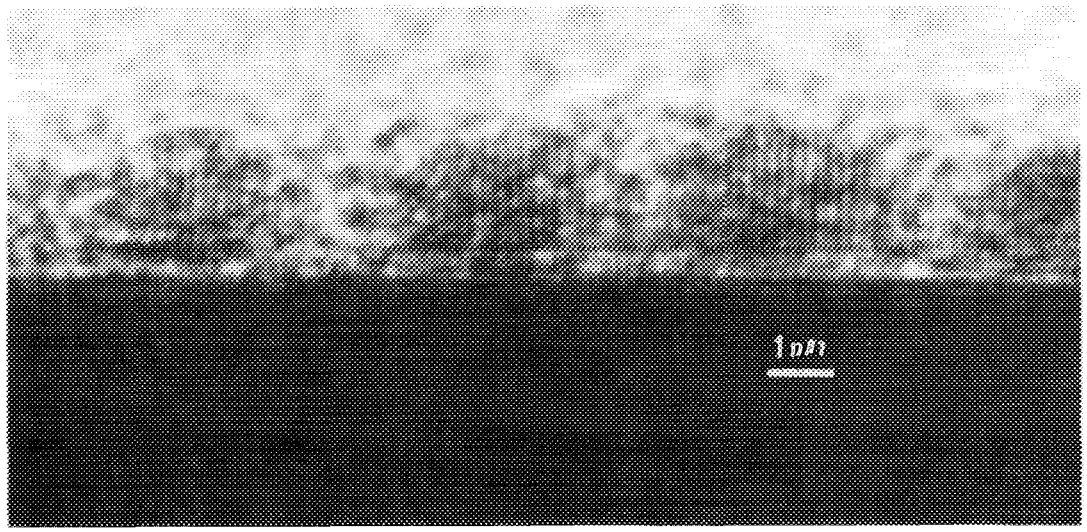

FIG. 2. High-resolution image of a particle annealed in O_2 at 10^{-7} Torr.

is not obvious. Indeed, the particle seems to be buried in the substrate. Particles were selected to measure the lattice parameter from the interface to the top. The average measurements are shown in Fig. 5. As the interface is not well defined, the last layer with a distance of 0.21 nm from the substrate towards the particle is tentatively taken as the first Pd layer at the interface. Further, the lattice parameter decreases again to 1.02 times the bulk value of the Pd. Then, the lattice parameter increases up to a larger value: it is 0.215 nm near the top of the particle. It was previously shown from simulations with the multislice method that the observed dilatation near the top was an HRTEM artifact (22). However, the measured dilatation is larger than that corresponding to the artifact. In fact, this large dilatation could be due to the first stage of the formation of the PdO around the particle.

Figure 6a illustrates Pd particles with the PdO lattice clearly visible on the surface and on the edges. In Fig. 6b, the smallest particle (<2 nm) at the center of the image has been completely oxidized to PdO. Here, the PdO is seen with its (001)PdO face parallel to the (001)MgO and the [100]PdO direction parallel to [100]MgO, in order that the two sets of lattice fringes (101) are visible in the profile view. The lattice distance $d_{(101)}$ of PdO is 0.264 nm, which is larger than the distance $d_{(200)}$ of Pd by 35% and larger than the distance $d_{(111)}$ of Pd by 18%. Hence the presence of PdO cannot be confused with Pd in another orientation.

Annealing Under Hydrogen

The same type of measurement was made with particles annealed in H_2. The shape is not modified compared to

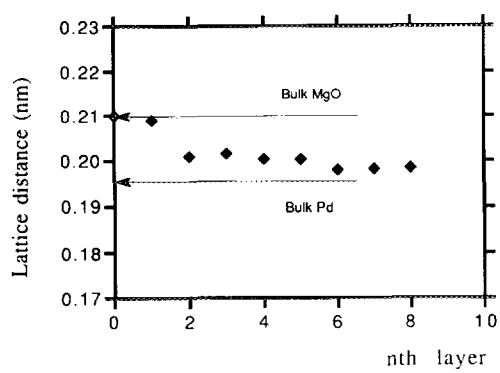

FIG. 3. Average distance between the (200) lattice planes of Pd annealed in O_2 at 10^{-7} Torr, normal to the interface, in the successive layers from the interface with MgO (layer 1) until the eighth layer.

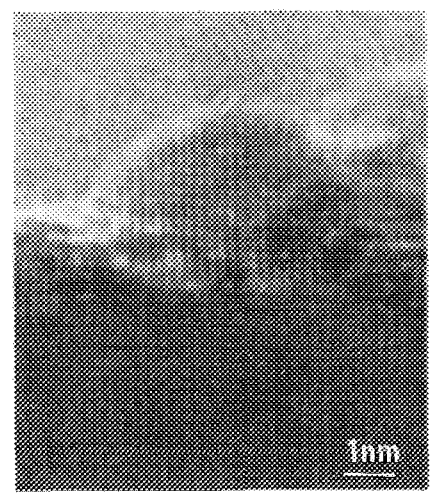

FIG. 4. HRTEM image of a Pd particle annealed in O_2 at 10^{-1} Torr.

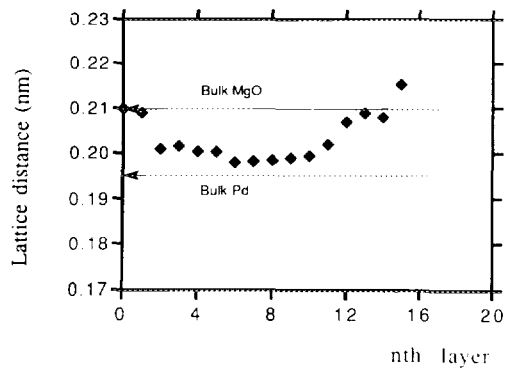

FIG. 5. Average distance between the (200) lattice planes of Pd annealed in O_2 at 10^{-1} Torr, normal to the interface, in the successive layers.

the particles annealed in vacuum. Figure 7 is the high-resolution image of a particle annealed at 10^{-7} Torr of hydrogen showing that the interface is flat. The variations of the lattice parameter in the successive palladium layers from the interface are represented in Fig. 8. From the third layer, the average lattice distance is dilated by 3–4% relative to the bulk Pd. With such a dilatation, the lattice parameter is close to that of PdH of *fcc* structure with $d_{(200)} = 0.201$ nm.

Particles annealed in H_2 at "high" pressure (10^{-1} Torr) give approximately the same results; the Pd lattice is expanded as in the case of annealing in H_2 at 10^{-7} Torr. However, the phase diagram of the Pd–hydrogen system (23) indicates that bulk palladium hydride is not stable under our conditions (temperature and pressure) during annealing of the particles.

DISCUSSION

As described above, Pd particles (4–5 nm in size), epitaxially grown on MgO (001) microcubes in UHV, were annealed in O_2 or H_2 at pressures of 10^{-1} and 10^{-7} Torr. Particles annealed in UHV have a half-octahedron shape limited by 4 (111) planes and truncated at the top by a (100) plane, and their lattice is dilated by ~1.8% (21). Annealing in H_2 and O_2 influences the lattice parameter of the Pd particles. However, their shape is only transformed significantly after annealing in O_2. The stronger adsorption of oxygen, resulting in a larger decrease of the surface tension, can explain this difference. The decrease of the surface tension of an (*hkl*) face is $\Delta\sigma(hkl) = E_{ad} \times n_s$ is the density of adsorbed molecules and E_{ad} is the adsorption energy of the gas molecules (or atoms in the case of dissociative adsorption), as given in the literature (24, 25). For H_2 adsorption, the values of E_{ad} are 88–99, 91–102, and 96–102 kJ/mol for the (111), (100), and (110) surfaces, respectively. The number of adsorbed hydrogen atoms, calculated from the coverage at equilibrium and taking a sticking coefficient of 0.12, is given in Table 1.

In the case of annealing in H_2, even at the pressure 10^{-1} Torr, the coverage is smaller than 10^{-4} on all the considered faces; therefore the variation of the surface tension is negligible (see Table 2) and does not modify the morphology of the particles.

For oxygen, the adsorption energies are much larger: 230, 250, and 334 kJ/mol for the (111), (100), and (110) faces, respectively. Taking a sticking coefficient of 0.25 for the (111) faces and 0.4 for the (100) face (27), the oxygen coverage is calculated (see Table 1). In the case of annealing at 450°C, in 10^{-1} Torr of O_2, the saturation coverage is always obtained, and at the lower pressure of 10^{-7} Torr the oxygen coverage is about 0.5 monolayer. In the last case, the calculated variation of surface tension $\Delta\sigma$ is -1.2 J/m^2 on the (111) faces. It is of the same order as the surface tension σ_{111} on bulk Pd (1.7 J/m^2). For more open surfaces the adsorption energy is higher and the resulting coverage is also larger. Annealing in O_2 must decrease the anisotropy of the surface energy, so even at

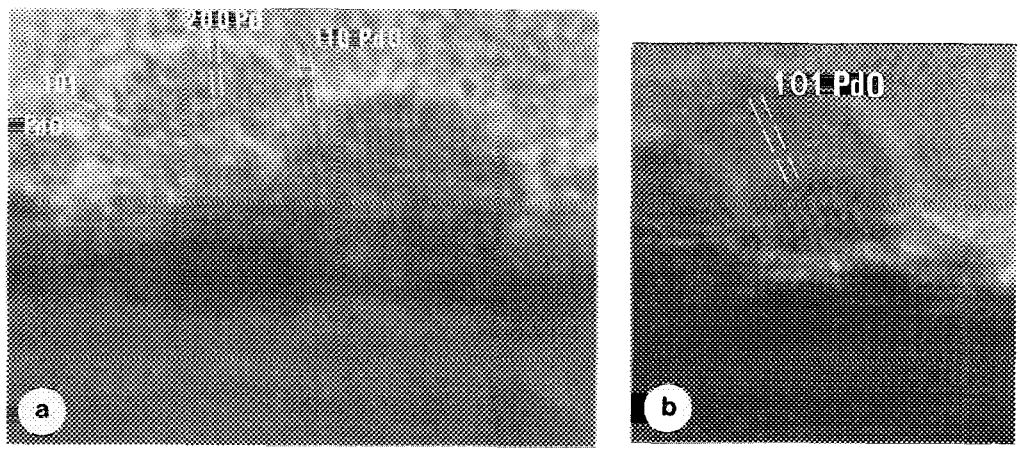

FIG. 6. (a) Pd particles with PdO growing around; (b) PdO particle seen normally to the (010) face.

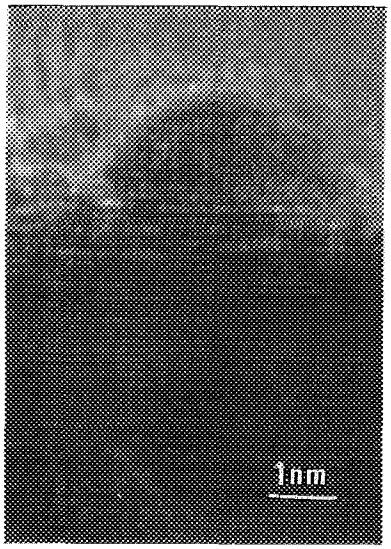

FIG. 7. HRTEM image of a Pd particle annealed in H_2 at 10^{-7} Torr.

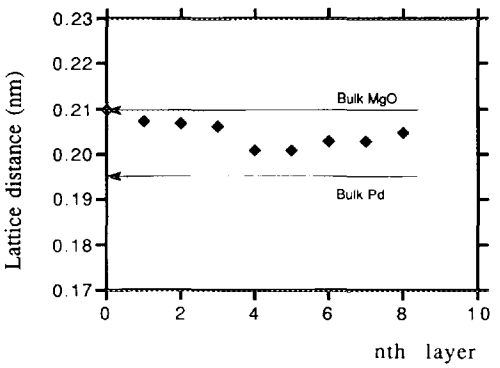

FIG. 8 Average distance between the (200) lattice planes of Pd annealed in H_2 at 10^{-1} Torr, normal to the interface, in the successive layers.

10^{-7} Torr it favors the formation of high order crystallographic faces. This can explain why particles annealed at 10^{-1} Torr are completely rounded.

In both cases of annealing, either at 10^{-7} or 10^{-1} Torr, the particles become rounded but they are not flattened as previously reported in Refs. (13, 14).

Both annealings in H_2 and O_2 induce variations of the lattice parameter of the Pd particles. In the case of annealing in H_2, the lattice parameter of 4 to 5-nm-sized particles is expanded by 3–4%. With such an expansion, the lattice is close to that of Pd β-hydride, although it might not be stable under these conditions of H_2 pressure. However, for annealing of such particles in UHV, we observed dilatations of 2.7% (22). Therefore, after H_2 annealing, a slightly larger expansion is observed, but the difference is too small to prove the formation of Pd hydride. No additional information is obtained by HRTEM because both structures are identical.

A recent paper (26) reports an expansion of 2.5% for Pd particles (<4 nm) deposited on amorphous carbon, SiO_2, or alkali halides, in vacua of 10^{-9} Torr or 10^{-8} Torr, or exposed to H_2O at 10^{-5} Torr. This dilatation vanishes in the case of a continuous layer of Pd. The authors explain this dilatation as a partial formation of the Pd hydride in the particles, due to the decomposition of H_2O or residual hydrogen (23).

If the hypothesis of hydride formation even in UHV was true, we should observe a maximum dilatation of about 3% compared to β-PdH. To explain the 8% dilatation of 2-nm Pd clusters which we observed (21), it is necessary to advance another mechanism, namely pseudomorphism.

EXAFS measurements have provided evidence for the formation of PdH with 1- to 4-nm-sized Pd clusters (28). However, this hydride formation was reversible and only appeared at high pressure (= 500 Torr). It seems reasonable to think that under our conditions ($P_{H_2} < 10^{-1}$ Torr) Pd hydride is not formed, but we cannot rule out the

TABLE 1

Calculated Number of Adsorbed Atoms per cm² (n_s) on the Different Crystallographic Faces of Pd, as a Function of H_2 and O_2 Pressures

	No. of adsorbed atoms per cm²			
	Hydrogen		Oxygen	
Crystal face	10^{-7} Torr pressure	10^{-1} Torr pressure	10^{-7} Torr pressure	10^{-1} Torr pressure
Pd(111)	1.22×10^{5}	1.22×10^{11}	0.32×10^{15}	$0.32 \times 10^{21} > n_s$(max)
Pd(100)	4.7×10^{5}	4.7×10^{11}	0.78×10^{15}	$0.78 \times 10^{21} > n_s$(max)
Pd(110)	4.7×10^{5}	4.7×10^{11}	0.78×10^{15}	$0.78 \times 10^{21} > n_s$(max)

Note. n_s(max) corresponds to the saturation coverage.

TABLE 2

Calculated Variations of the Surface Energy $\Delta\sigma$ (J/m^2) for Different Crystallographic Faces of Pd, Due to the Adsorption of H_2 and O_2

	Surface energy (J/m^2)			
	In Hydrogen		In Oxygen	
Crystal face	10^{-7} Torr pressure	10^{-1} Torr pressure	10^{-7} Torr pressure	10^{-1} Torr pressure
Pd(111)	1.95×10^{-10}	1.9×10^{-4}	1.2	3.8
Pd(100)	8.8×10^{-10}	8.8×10^{-4}	3.2	4.16
Pd(110)	8.8×10^{-10}	8.8×10^{-4}	4.36	5.56

possibility of diffusion of hydrogen atoms inside the Pd lattice which could result in an additional dilatation.

Annealing in O_2 at 10^{-7} Torr weakly modifies the lattice parameter by 2%. This expansion is very close to the dilatation of the 4- to 5-nm particles annealed in UHV (21), which is mainly due to pseudomorphism. At 10^{-1} Torr, the lattice expansion is larger on the top of the particles, and it certainly corresponds to the beginning of formation of the oxide PdO. The first stage of formation of PdO can only be observed on the surface on the high-resolution images. It does not diffuse to the center of the clusters except for one small isolated particle of ~1.5 nm which was completely transformed into PdO.

Our results are different from those obtained for Pd particles on TiO_2 heated in air at 500°C (29). The authors in that case have measured an increase of the Pd lattice by 15%, but stoichiometric PdO was only observed in a few cases. They suggest that the deformations and expansions of the Pd lattice annealed in air is due to the interaction between the Pd and the TiO_2 substrate.

The oxidation at 800°C of Pd particles deposited on MgO and exposed to a residual pressure of 10^{-7} Torr has been studied (17). The particles were first surrounded by a 1-nm-thick PdO layer, then, after complete oxidation, PdO was found in epitaxial (110) orientation on MgO(100). No intermediate microstructural phase was found before the complete oxidation. PdO was also produced by very strong irradiation of Pd films in an electron microscope (30). Under our conditions of observation, the oxidation cannot be due to the effect of the electron beam. Our experiments show that even at 450°C, at 10^{-1} Torr, the oxidation starts near the surface of the particles.

REFERENCES

1. Wulff, G., *Z. Kristallogr. Mineral.* **34,** 449 (1901).
2. Wang, S. W., Falicov, L. M., and Searcy, A. W., *Surf. Sci.* **143,** 609 (1984).
3. Marks, L. D., *Surf. Sci.* **150,** 358 (1985).
4. Shi, A. C., *Phys. Rev. B* **36,** 9068 (1987).
5. Wang, T., Lee, C., and Schmidt, L. D., *Surf. Sci.* **163,** 181 (1985).
6. Schmidt, L. D., Wang, T., and Vacquez, A., *Ultramicroscopy* **8,** 175 (1982).
7. Harris, P. J. F., *Surf. Sci. Lett.* **185,** L 459 (1987).
8. Harris, P. J. F., *Nature* **323,** 792 (1986).
9. Rickard, J. M., Genovese, L., Moata, A., and Nitsche, S., *J. Catal.* **121,** 141 (1990).
10. Shi, A. C., and Masel, R. I., *J. Catal.* **120,** 421 (1989).
11. Smith, D. J., *J. Catal.* **81,** 107 (1983).
12. Lee, W. H., Vanloo, K. R., Petrova, V., Woodhouse, J. B., Loxton, C. M., and Masel, R. I., *J. Catal.* **126,** 658 (1990).
13. Heinemann, K., Osaka, T., and Poppa, H., *Ultramicroscopy* **12,** 9 (1983).
14. Heinemann, K., Osaka, T., Poppa, H., and Avalos-Borja, M., *J. Catal.* **83,** 61 (1983).
15. Doering, D. L., Poppa, H., and Dickinson, J. T., *J. Catal.* **73,** 104 (1982).
16. Gillet, M. F., and Channakhone, S., *J. Catal.* **97,** 427 (1986).
17. Ou, H. J., and Cowley, J. M., *Phys. Status. Solidi A* **107,** 719 (1988).
18. Baker, R. T. K., Prestridge, E. B., and McVicker, G. B., *J. Catal.* **89,** 422 (1984).
19. Lamber, R., Jaeger, N., and Schulz-Ekloff, G., *J. Catal.* **123,** 285 (1990).
20. Erlandsson, G., Eriksson, M., Olsson, L., Helmersson, U., Lundstrom, I., and Petersson, L. G., *J. Vac. Sci. Technol., B* **9,** 825 (1991).
21. Giorgio, S., Henry, C. R., Chapon, C., and Penisson, J. M., *J. Cryst. Growth* **100,** 254 (1990).
22. Giorgio, S., Chapon, C., Henry, C. R., and Nihoul, G., *Philos. Mag. B* **67**(6), 773 (1993).
23. Wicke, E., and Brodowsky, H., "Topics in Applied Physics, Vol. 29: Hydrogen in Metals II" (G. Alefeld and J. Volkl, Eds.). Springer-Verlag, Berlin, 1978.
24. Conrad, H., Ertl, G., and Latta, E. E., *Surf. Sci.* **41,** 435 (1974).
25. Behm, R. J., Christmann, K., and Ertl, G., *Surf. Sci.* **99,** 320 (1980).
26. Kuhrt, C., and Anton, R., *Thin Solid Films* **198,** 301 (1991).
27. Stuve, E. M., Madix, R. J., and Brundle, C. R., *Surf. Sci.* **146,** 155 (1984).
28. Moraweck, B., Clugnet, G., and Renouprez, A., *J. Chim. Phys. Phys.-Chim. Biol.* **83,** 265 (1986).
29. Jacobs, J. W. M., and Schryvers, D., *J. Catal.* **103,** 436 (1987).
30. Ye, H. Q., Ning, X. G., and Smith, D. J., *Surf. Sci.* **250,** 90 (1991).